Article

Synergistic Evolution of Palaeoenvironment—Bionts and Hydrocarbon Generation of Permian Saline Lacustrine Source Rocks in Jimusar Sag, Junggar Basin

Zaibo Xie [1,2,3], Huifei Tao [1,2,*], Yongqiang Qu [4], Tao Wu [5], Dongzheng Ma [1,2,3], Tianhai Wang [1,2,3], Zhen Qin [1,2,3], Long Su [1,2] and Zhongping Li [1]

1 Oil and Gas Research Center, Northwest Institute of Eco-Environment and Resources, Chinese Academy of Sciences, Lanzhou 730000, China
2 National Engineering Research Center of Offshore Oil and Gas Exploration, Beijing 100027, China
3 University of Chinese Academy of Sciences, Beijing 100049, China
4 Northwest Branch of PetroChina Research Institute of Petroleum Exploration and Development, Lanzhou 730000, China
5 Research Institute of Exploration and Development, Petrochina Xinjiang Oilfield Company, Karamay 834000, China
* Correspondence: tophic3@yeah.net

Abstract: This study focused on Middle Permian Lucaogou Formation saline lake source rocks, utilizing a combination of biomarkers and hydrocarbon generation thermal simulation to analyze their biological compositions, depositional environments, and hydrocarbon generation potential. The Pr/Ph ratio, Ph/nC_{18} ratio, and Pr/nC_{17} ratio indicate that the Lucaogou Formation was in a reducing environment during the deposition period, and the lower part of the Lucaogou Formation (P_2l_1) is more anoxic than the upper part of the Lucaogou Formation (P_2l_2). The maturity index 20S (%) and ββ (%) reflect that the maturity of organic matter in the P_2l_1 is slightly higher than that in the P_2l_2. The G/H index and the ETR index indicate that the stratification of the water column is better during the sedimentary period of Lucaogou Formation and the salinity of the P_2l_1 is higher than that of the P_2l_2. The biomarker parameters of nC_{21-}/nC_{22+}, CPI, S/H, and $C_{22}T/C_{21}T$ reflect that the organic matter of the source rocks have a higher abundance of bacteria and algae than higher plants, and the contents of bacteria are more than that of algae. The (7- + 8-MMAs)/C_{max} and $(C_{28} + C_{29} - St)/St$ parameters indicate that cyanobacteria accounted for a certain proportion of bacteria, and the algae are mainly green algae. The co-evolution of the sedimentary environment and the biological composition reflects the control of the sedimentary paleoenvironment on biological composition. According to the relative content of cyanobacteria, green algae, and Rhodophyta, the source rocks of the upper and lower Lucaogou Formation correspond to the low-salinity type (LS-type) and the high-salinity type (HS-type), respectively. Compared with LS-type source rocks, HS-type source rocks have greater generation potential of oil and weaker gas generation potential. This study is valuable for the accurate assessment of source rocks and holds significant practical implications for the exploration of oil and gas resources.

Keywords: biomarker; synergistic evolution; hydrocarbon generation; Lucaogou Formation; Jimusar

1. Introduction

The source of organic matter and its accumulation in lacustrine source rocks are key factors that control hydrocarbon generation and are important to assess during the exploration and evaluation of oil and gas resources [1]. Therefore, it is very important to find out the controlling factors of the biological source of organic matter in saline lake source rocks. The biogenesis of organic matter in rocks has always been significant research content in petroleum geology and organic geochemistry [2–5]. Due to the sensitivity of

organic matter sources to environmental changes [4], lacustrine source rocks generally show strong lateral and vertical heterogeneity [6]. Previous studies have summarized the formation of source rocks and the enrichment of organic matter in ancient lakes under different tectonic settings and paleoenvironments [7], such as the Green River Formation type, the middle-deep lake type [8], the shallow lake type [9], and the anoxic lake model [10]. Specifically, the synergistic evolution of the sedimentary paleoenvironment and the source rock organic matter [5] may cause differences in the hydrocarbon generation potential of source rocks.

Different researchers have carried out in-depth research on the controlling factors of organic matter accumulation and petroleum generation. It is generally believed that the main controlling factors are as follows: (i) the strength of primary productivity is particularly important for the accumulation of organic matter and (ii) the abundance of organic matter in source rocks is determined by the preservation conditions [11–14]. Changes in the paleoenvironment directly affect the characteristics of the biological community, the depth of the lake, the salinity of the water body, and the paleo-oxygenation facies of the lake [15,16], which also influences the type, enrichment, and preservation of the organic matter. The geochemical characteristics of the source rock record paleoenvironmental signatures, which indicates the source of the organic matter. Many shales that are sources of the hydrocarbons trapped in the oil reservoir in northwestern China, such as the Fengcheng Formation (P_1f) in the Mahu Sag and the Lucaogou Formation (abbreviation is P_2l) in the Jimusar Sag, are associated with volcanic-hydrothermal activities [7,17,18]. Volcanic ash and hydrothermal activities bring large amounts of nutrients that stimulate the development of phytoplankton and cyanobacteria [19,20].

Previous studies have extensively investigated the elements and organic geochemistry in the Lucaogou Formation and have identified differences between its upper and lower parts [9,21,22]. However, the biomarker characteristics of the source rocks remain poorly researched; notably, the sedimentary paleoenvironment of the P_2l and the biological origin of the organic matter. There has been limited quantitative research through the use of temperature and pressure simulation experiments. The aim of this paper is to investigate the variation in the hydrocarbon generation potential of organic matter derived from various biological sources. Additionally, we will explore the co-evolution trend between the evolution of paleoenvironments and biological sources. To achieve this, we will conduct organic geochemical analyses and temperature–pressure simulation experiments to quantitatively analyze the differences in hydrocarbon generation among various source rocks resulting from environmental changes. Firstly, with emphasis on the co-evolution of the organic matter source and the environment, the characteristics and differences in the source rocks from the upper and lower parts of the Lucaogou Formation (abbreviation is P_2l_2 and P_2l_1) will be analyzed by organic geochemical analyses; for instance, the maturity, the formation environments, the enrichment factors, and the evolution pattern of the organic matter. Secondly, the coupled simulation experiments in high temperature and pressure will be used to analyze the hydrocarbon generation differences (the potential of oil and gas generation) between the source rocks of the P_2l_2 and the P_2l_1. Finally, the organic geochemical characteristics and the coupling simulation experiment data will be combined in order to comprehensively evaluate the source rocks of the P_2l_2 and the P_2l_1.

2. Geological Setting

The Junggar Basin is located in northwest China (Figure 1a), and the Jimusar Sag is located in the eastern uplift of the Junggar Basin [18] (Figure 1b). Based on the division of the tectonic units in the Junggar Basin, the Jimusar Sag belongs to the second-order tectonic unit, affected by Hercynian, Indosinian, Yanshan, and Himalayan multistage tectonic movements successively [22]. In the interior of the depression, subsidence has occurred in each tectonic movement period, and the periphery was surrounded by Shaqi uplift, Guxi uplift, Beisantai uplift, and the Fukang fault zone, with obvious boundaries (Figure 1c).
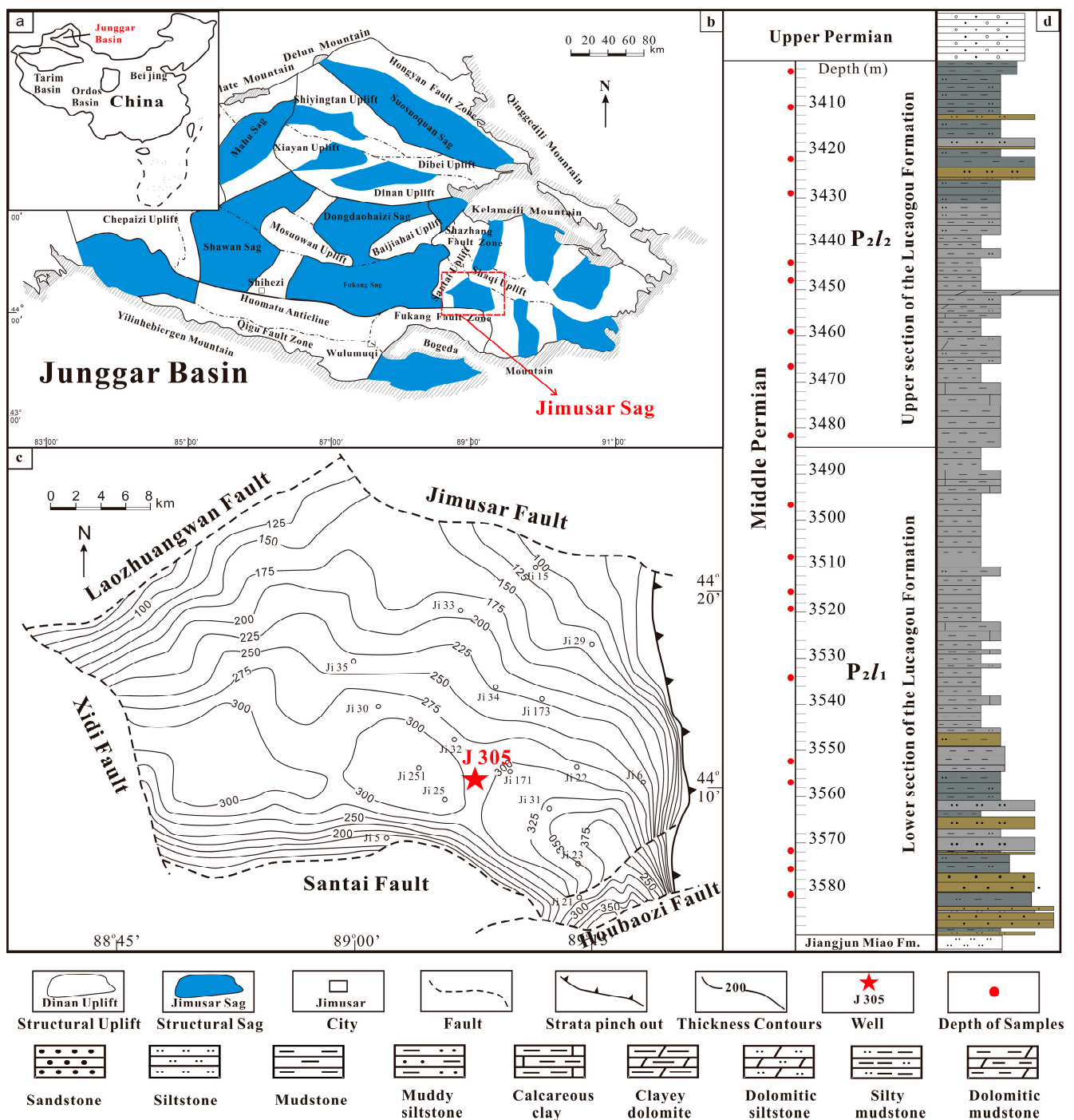
Figure 1. Location and column-map sampling points of Well J305. (**a**) Location of Junggar Basin on a map of China. (**b**) Sag distribution map of Junggar Basin. (**c**) Contour map of sedimentary thickness of Lucaogou Formation in Jimusar Sag (Adapted with permission from Ref. [23]). (**d**) Lithology and sampling points of Well J305 (modified with reference [24]).

Permian strata in the Jimsar sag successively developed the Jiangjunmiao Formation, the Lucaogou Formation, and the Wutonggou Formation, from bottom to top [22]. Among those strata, the Permian Lucaogou Formation (P_2l) is the primary strata for shale oil exploration, which is developed in the inland lake environment under the sutures of the Tarim plate and the Junggar plate, dominated by semi-deep lacustrine facies [25,26]. The thickness of the P_2l is 200~300 m, and it develops siltstone mudstone, mudstone, shale, and

tuffaceous dolomite with thin tuff, which are the major source rock series in the Jimusar Sag [27].

The Lucaogou Formation (P_2l) is divided into two parts: the lower part (P_2l_1) and the upper part (P_2l_2), according to logging data and lithology characteristics [18] (Figure 1d). In Well J305, the depth of the P_2l_1 is from 3486 to 3598 m, while that of the P_2l_2 ranges from 3402 to 3486 m. The reservoir mainly consists of the following three types of rock: dolomite siltstone, tuffaceous siltstone, and tuffaceous dolomite [27]. The organic-rich shales interbedded with the reservoir in the "sweet spot" member are the main source rocks and reach maturity at the "oil-generating window". The source rocks of the lower Lucaogou Formation may have good oil-generation potential [27]. They are currently in a massive oil generation stage, forming a source–reservoir symbiosis and a proximal accumulation mode. These reservoirs are targets for shale oil exploration [22].

The burial history of the Jimusar sag is shown in Figure 2. After the deposition of the Lucaogou Formation, it underwent rapid and continuous subsidence. At the end of the Triassic, the strata experienced regional tectonic uplift, but the Lucaogou Formation did not erode at the surface. At the end of the Jurassic, small-scale uplift and denudation had little effect on the evolution of the organic matter in the Lucaogou Formation. Due to regional tectonic movement, the strata began to uplift in the late Cretaceous, and the Cretaceous strata were eroded. At this time, the source rocks of the Lucaogou Formation were within the hydrocarbon generation threshold. The strata were buried again in the late Cretaceous. Furthermore, the present burial depth is the maximum burial depth of the strata [28]. According to vitrinite reflectance (Ro) characteristics, it is mainly distributed in a range of 0.7% to 1.0 %, indicating that the source rock evolution is in a stage of low maturity [29,30]. The paleogeothermal gradient at the end of the Permian was about 36.3 °C/km [31], while the current geothermal gradient ranges from 27.5 to 35 °C/km [32].
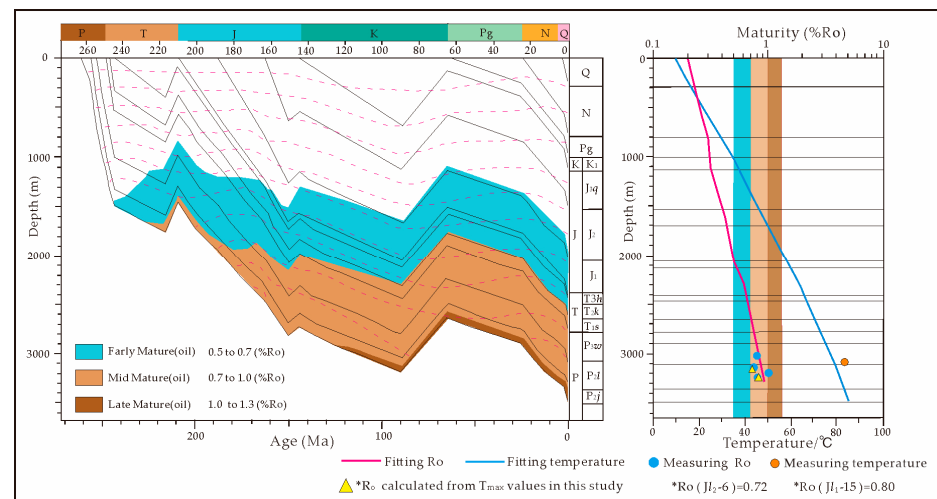

Figure 2. Burial and thermal history of P_2l in the Jimusar Sag (Adapted with permission from Ref. [28]). *Ro = 0.018 × T_{max} − 7.16 (Reprinted with permission from Ref. [29]).

3. Samples and Experiments

3.1. Samples

Nineteen core samples were selected from Well J305 in the Jimusar Sag, Junggar Basin. The lithology of the samples is mudstone of the Lucaogou Formation (sample No.: Jl_2-1~Jl_1-19, Table 1 and Figure 1). Two samples (mudstone, Jl_2-6 (*R_O = 0.72) and Jl_1-15 (*R_O = 0.80)) were selected for the hydrocarbon generation simulation experiment. Samples Jl_2-6 and Jl_1-15 represent typical source rocks in the P_2l_2 and P_2l_1, respectively. The above two samples were crushed to −80 mesh and extracted with dichloromethane to remove soluble organic matter, which needs to be removed before the temperature–pressure simulation experiments.

Table 1. Biomarker parameters of source rocks within the Middle Permian Lucaogou Formation in the Jimusar Sag, Junggar Basin.

Stratum	Sample No.	Depth (m)	Lithology	TOC (%) *	Pr/Ph	nC_{21-}/nC_{22+}	G/H *	S/H	20S (%) *	ββ (%) *	ETR *	$C_{22}T/C_{21}T$	27%	28%	29%	$(C_{28} + C_{29} - St)/St$	(7- + 8-C_{18} MMAs)/Cmax *	$2\alpha - C_{32}Meh/C_{32}H$ *
P₂l₂	Jl₂-1	3402	Mudstone	6.02	1.00	1.56	0.16	0.09	0.39	0.19	0.57	0.10	34%	22%	44%	0.66	9.29%	5.17%
	Jl₂-2	3410	Mudstone	7.30	0.93	1.61	0.17	0.10	0.39	0.18	0.47	0.10	36%	22%	42%	0.64	9.53%	5.01%
	Jl₂-3	3422	Mudstone	4.36	1.00	0.77	0.19	0.16	0.36	0.18	0.65	0.10	30%	26%	44%	0.70	6.32%	4.95%
	Jl₂-4	3430	Mudstone	5.02	0.93	1.62	0.20	0.18	0.37	0.18	0.58	0.10	34%	27%	39%	0.66	8.88%	4.25%
	Jl₂-5	3446	Mudstone	5.50	0.80	4.79	0.25	0.18	0.46	0.26	0.52	0.12	19%	37%	45%	0.81	9.42%	4.42%
	Jl₂-6	3450	Mudstone	5.94	0.90	0.51	0.22	0.22	0.36	0.20	0.75	0.11	29%	34%	37%	0.71	3.55%	5.33%
	Jl₂-7	3462	Mudstone	3.70	0.96	1.12	0.35	0.13	0.39	0.16	0.74	0.11	18%	34%	48%	0.82	7.16%	5.32%
	Jl₂-8	3470	Mudstone	2.83	0.88	0.77	0.22	0.36	0.37	0.18	0.66	0.11	26%	32%	42%	0.74	8.09%	5.34%
	Jl₂-9	3486	Mudstone	3.45	0.62	1.07	0.18	0.25	0.43	0.24	0.89	0.15	10%	36%	54%	0.90	11.60%	5.72%
	Average of P₂l₂			4.90	0.89	1.54	0.22	0.19	0.39	0.20	0.65	0.11	26%	30%	44%	0.08	8.20%	5.06%
P₂l₁	Jl₁-10	3498	Mudstone	6.08	0.68	2.61	0.24	0.26	0.43	0.21	0.87	0.12	11%	40%	49%	0.89	17.78%	5.96%
	Jl₁-11	3510	Mudstone	2.66	0.72	2.91	0.30	0.48	0.43	0.23	0.80	0.13	5%	34%	61%	0.95	18.04%	7.30%
	Jl₁-12	3518	Mudstone	7.55	0.63	3.29	0.18	0.42	0.43	0.21	0.88	0.12	18%	37%	45%	0.82	15.82%	5.63%
	Jl₁-13	3522	Mudstone	3.30	0.48	0.71	0.22	0.27	0.44	0.25	0.93	0.15	11%	35%	54%	0.89	13.65%	5.68%
	Jl₁-14	3538	Mudstone	3.19	0.46	0.66	0.26	0.45	0.45	0.24	0.87	0.14	8%	35%	57%	0.92	17.66%	5.67%
	Jl₁-15	3554	Mudstone	6.20	0.82	5.30	0.25	0.30	0.44	0.24	0.80	0.13	10%	35%	55%	0.90	14.64%	6.92%
	Jl₁-16	3562	Mudstone	7.58	0.85	4.10	0.26	0.25	0.45	0.26	0.72	0.13	8%	37%	55%	0.92	16.21%	6.25%
	Jl₁-17	3578	Mudstone	9.21	0.86	3.85	0.26	0.24	0.44	0.26	0.70	0.14	8%	37%	56%	0.92	15.00%	6.39%
	Jl₁-18	3582	Mudstone	5.15	0.72	0.82	0.21	0.24	0.44	0.26	0.75	0.14	10%	34%	56%	0.90	14.89%	6.05%
	Jl₁-19	3586	Mudstone	8.30	0.62	0.91	0.23	0.26	0.46	0.27	0.79	0.15	9%	36%	55%	0.91	16.36%	6.48%
	Average of P₂l₁			5.92	0.69	2.52	0.24	0.32	0.44	0.24	0.81	0.14	10%	36%	54%	0.16	16.01%	6.23%

Note: TOC = Total organic carbon (wt%); Pr/Ph = Pristane/Phytane; nC_{21-}/nC_{22+} = Short-chain *n*-alkanes (C_{21}-)/Long-chain *n*-alkanes (C_{22}+); S/H = Stetane/Hopane; 20S (%) = C_{29}sterane $\alpha\alpha\alpha$20S/(20S + 20R); ββ (%) = C_{29}sterane $\alpha\beta\beta/(\alpha\beta\beta + \alpha\alpha\alpha)$; ETR = $(C_{28} + C_{29})/(C_{28} + C_{29} + Ts)$; $C_{22}T/C_{21}T$ = C_{22} tricyclic terpane/C_{21} tricyclic terpane; 27% = C_{27}steranes/(C_{27}steranes + C_{28}steranes + C_{29}steranes); 28% = C_{28}steranes/(C_{27}steranes + C_{28}steranes + C_{29}steranes); 29% = C_{29}steranes/(C_{27}steranes + C_{28}steranes + C_{29}steranes); $(C_{28} + C_{29}$-St)/St = (C_{28} sterane + C_{29}sterane)/(total sterane); (7- + 8-MMAs)/C_{max} = (7- + 8-C_{18} Monomethylalkanes)/Maximum *n*-alkane; $2\alpha - C_{32}$Meh/C_{32}H = $2\alpha - C_{32}$ methylhopanoids/C_{32} hopanoids (%). The data with '*'are adapted with permission from Ref. [24].

3.2. Experiments

The experiments involved in this study mainly include two parts: the organic geochemical analyses and the hydrocarbon generation simulation experiments.

3.2.1. Organic Geochemistry Experiments

Th organic geochemistry experiments consisted of the determination of TOC (total organic carbon) content, Soxhlet extraction and separation, and GC–MS of saturated hydrocarbons. The determination of TOC was completed with a Leco CS230 carbon sulfur analyzer, using the standard GB/19145-2003. The Soxhlet method was used to extract and separate soluble organic matter from the samples. The purpose of extraction and separation was to obtain asphaltenes, non-hydrocarbons, aromatic hydrocarbons, and saturated hydrocarbons of organic matter in the samples for further testing and analysis. Firstly, more than 60 g of the sample was weighed with a balance, and it was crushed to >100 mesh. The crushed sample was wrapped in filter paper and placed in an extractor. An excess of the extract (methanol and dichloromethane mixture, volume ratio 1:9) was added to the extractor for extraction for 72 h. Then, the extract was separated with a chromatographic column (silica gel: activated alumina = 3:1). Finally, saturated hydrocarbons (non-polar), aromatic hydrocarbons (weak polarity), resin (polarity), and asphaltenes (residues) were obtained by washing with *n*-hexane, dichloromethane, and methanol, respectively.

GC–MS (gas chromatography–mass spectrometry, GCMS-AP2020NX, SHIMADZU) was used to test the biomarkers. The GC–MS conditions were as follows: the inlet temperature: 280 °C; carrier gas: high-purity helium; carrier gas flow: 1.2 mL/min; chromatographic column: J & W.HP-5 (30 m × 0.25 mm × 0.25 μm) elastic quartz capillary column; temperature programmed: after 80 °C, 4 °C/min rose to 290 °C, constant temperature for 30 min; MS ion source: EI source; ion source temperature: 230 °C; quadrupole temperature: 150 °C; ionization energy of ion source: 70 eV; and scanning mode: full scanning.

3.2.2. The Thermal Simulation Experiments

Using the temperature compensation time principle, the thermal simulation experiment can effectively evaluate the hydrocarbon generation potential of source rocks [22,33]. The differences in the oil and gas generation behavior of the samples were compared, which provided an important theoretical basis revealing the mechanism of the oil and gas generation of source rocks and demonstrating their geochemical characteristics.

The semi-confined thermal simulation experiments were carried out using the WYMN-3 temperature–pressure simulator. Compared with the conventional closed experimental system, this instrument could effectively reduce the secondary cracking of heavy hydrocarbons and asphalt in the experimental process. It simulated the actual formation pressure of the rock samples by two axial pressures and interjected high pressure water to recreate the experimental simulation process under different fluid pressures. The principle of the experimental instruments is shown in Figure 3.

Based on the burial depth of the sample, the static rock pressure was set to 30 MPa in the experiment, and this constant value was maintained in the whole series of experiments. The initial fluid pressure was set to 30 MPa, and a pressure threshold of hydrocarbon expulsion fluid was set (this study was 2 MPa). When the actual fluid pressure was larger than 32 MPa during the experiment, a two-position three-way valve of the system was opened, and the generated hydrocarbons were discharged into a gas–liquid separator for storage. On the contrary, when the actual fluid pressure was lower than 28 MPa, the high-pressure pump valve was opened, and it injected deionized water. It was then closed when the fluid pressure reached 30 MPa.

Six target temperature points (300 °C, 350 °C, 375 °C, 400 °C, 450 °C, and 500 °C) were set in the simulation experiment. The simulation experiment at each temperature point rose to the target temperature over 3 h, and then kept constant for 72 h at the target temperature. After the temperature and pressure simulation experiment, the gas products of the experiment were collected using the saturated brine drainage gas collection method.

The non-hydrocarbon gas components of the gas products were analyzed with a MAT-271 high-resolution gas component mass spectrometer, and the hydrocarbon gas components (mainly $C_1 \sim C_5$) were analyzed with a GC-5890C gas chromatograph.
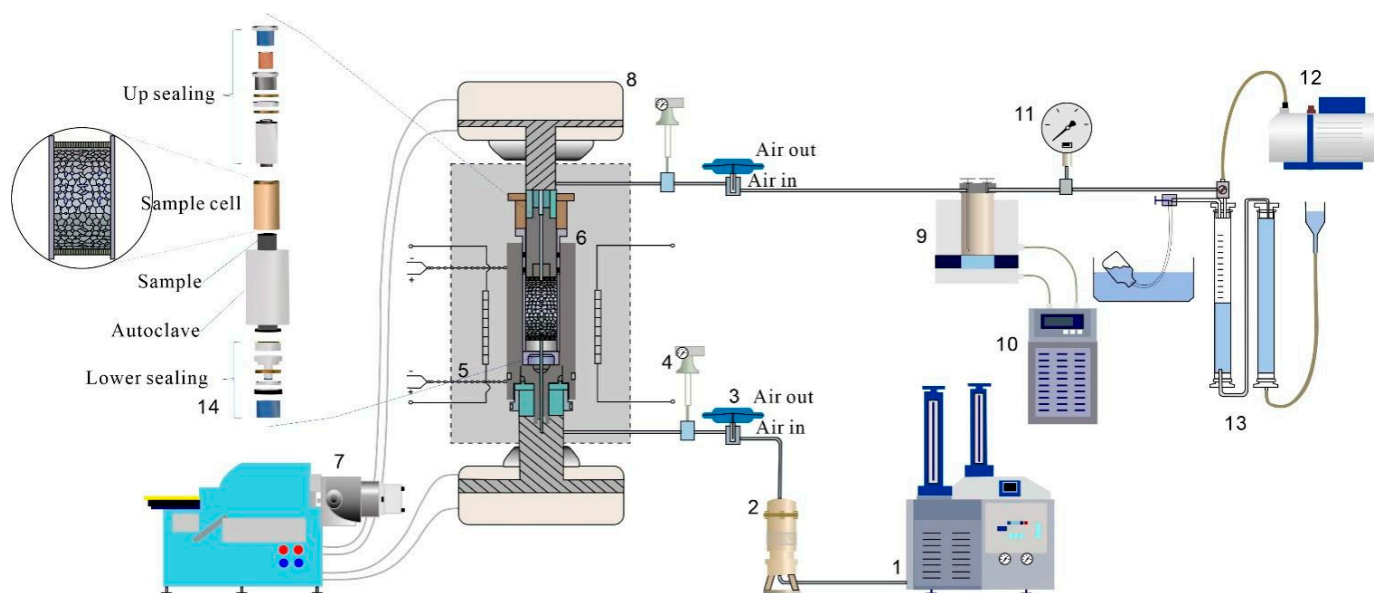

Figure 3. Schematic of the WYMN-3 HTHP thermal simulation equipment (Adapted with permission from Ref. [22]). 1—Pressure pump; 2—Pressure piston container; 3—Pneumatic valve; 4—Transmitter; 5—Thermocouple; 6—Autoclave; 7—Hydraulic pump; 8—Hydraulic cylinder; 9—Gas and liquid collector and cold trap; 10—Cooling water circulation machine; 11—Vacuum gauge; 12—Vacuum pump; 13—Drainage gas gathering device; 14—Sample cell and its sealing principle.

All experiments were completed in the Oil and Gas Research Center, Northwest Institute of Eco-Environment and Resources, Chinese Academy of Sciences.

4. Results

4.1. Organic Matter Abundance

The TOC values of the samples (Jl_1-10~Jl_1-19) from the P_2l_1 ranged from 2.6% to 9.2%, with an average value of 5.9%, while the TOC values of the samples (Jl_2-1~Jl_2-9) from the P_2l_2 ranged from 2.8% to 7.3%, with an average value of 4.9%. Overall, the TOC value from the P_2l_1 samples was higher than that from the P_2l_2 samples (Table 1; Figure 4).

4.2. Biomarkers

The biomarkers' distributive patterns of the extracts of the samples from the P_2l are shown in Figure 5. The distributive patterns of the *n*-alkanes in the samples of the P_2l were unimodal and the main peak was in the front, while the main peak of the P_2l_1 (Jl_1-10~Jl_1-19) samples was on the left side of the former. The characteristics of C_{29}, C_{28}, and C_{27} steranes in the P_2l_1 and P_2l_2 samples were also significantly different, being "sharp rise" and "slow rise", respectively.

4.2.1. *n*-Alkanes and Isoprenoid Alkanes

The distributive patterns of the *n*-alkanes and isoprenoid alkanes can be obtained with m/z 85 mass spectrometry, their related ratios and parameters can be used to analyze the source and the formation environment of sedimentary organic matter (Table 1; Figure 5). The (7- + 8-C_{18} Monomethyl alkanes)/Maximum *n*-alkane [(7- + 8-MMAs)/C_{max}] can be used to characterize cyanobacterial blooms [34–36]. The (7- + 8-MMAs)/C_{max} ranged from 0.04 to 0.18 (mean 0.12) (Table 1; Figure 6). The 7- + 8-MMAs and C_{max} were obtained with m/z 57 mass spectrum, and C_{max} represented the main peak of the *n*-alkanes. The

abundance of 7- + 8-MMAs in the samples was higher than its monomethyl homologues at 6-, 5-, 4-, 3-, and 2-, respectively.
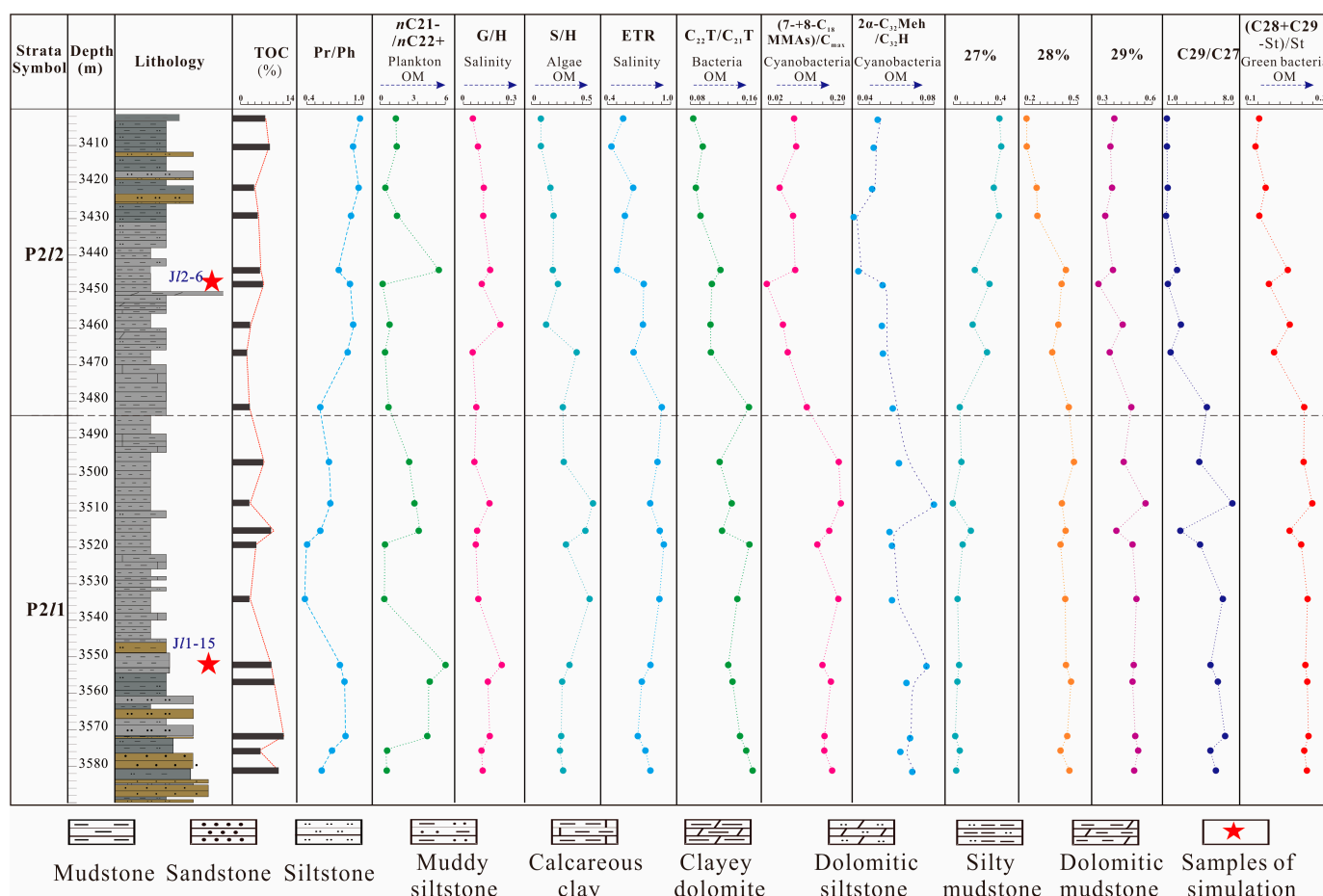

Figure 4. Variation of biomarker compound parameters of the Lucaogou Formation in Well J305 of the Jimusar Sag, Junggar Basin. Note: TOC = Total organic carbon (wt%); Pr/Ph = Pristane/Phytane; nC_{21-}/nC_{22+} = Short-chain *n*-alkanes (C_{21-})/Long-chain *n*-alkanes (C_{22+}); G/H = Gammacerane/$C_{30}\alpha\beta$ hopane; S/H = Stetane/Hopane; ETR = $(C_{28} + C_{29})/(C_{28} + C_{29} + Ts)$; $C_{22}T/C_{21}T$ = C_{22} tricyclic terpane/C_{21} tricyclic terpane; $(7- + 8-MMAs)/C_{max}$ = $(7- + 8-C_{18}$ Monomethylalkanes)/Maximum *n*-alkane; $2\alpha - C_{32}Meh/C_{32}H$ = $2\alpha - C_{32}$ methylhopanoids/C_{32} hopanoids (%); 27% = C_{27} steranes/(C_{27} steranes + C_{28} steranes + C_{29} steranes); 28% = C_{28} steranes/(C_{27} steranes + C_{28} steranes + C_{29} steranes); 29% = C_{29} steranes/(C_{27} steranes + C_{28} steranes + C_{29} steranes); C_{29}/C_{27} = C_{29} steranes/C_{27} steranes; $(C_{28} + C_{29}$-St)/St = (C_{28} sterane + C_{29} sterane)/(total sterane).

4.2.2. Terpanes

The relative abundance and distribution characteristics of terpanes can be obtained with the *m/z* 191 mass spectrum (Table 1; Figure 4). The ETR (extended tricyclic ratio, ETR = $(C_{28}TT + C_{29}TT)/(C_{28}TT + C_{29}TT + Ts)$) [37] ranged from 0.47 to 0.93 (average of 0.73), and the $C_{22}T/C_{21}T$ ratio (C_{22} tricyclic terpanes/C_{21} tricyclic terpanes) ranged from 0.10 to 0.15 (average of 0.12). C_{30} hopane was predominant in all of the samples. The ratio of 2α-methylhopane to hopanes ($2\alpha - C_{32}Meh/C_{32}H$) ranged from 4.25% to 7.30% (Table 1; Figure 5).
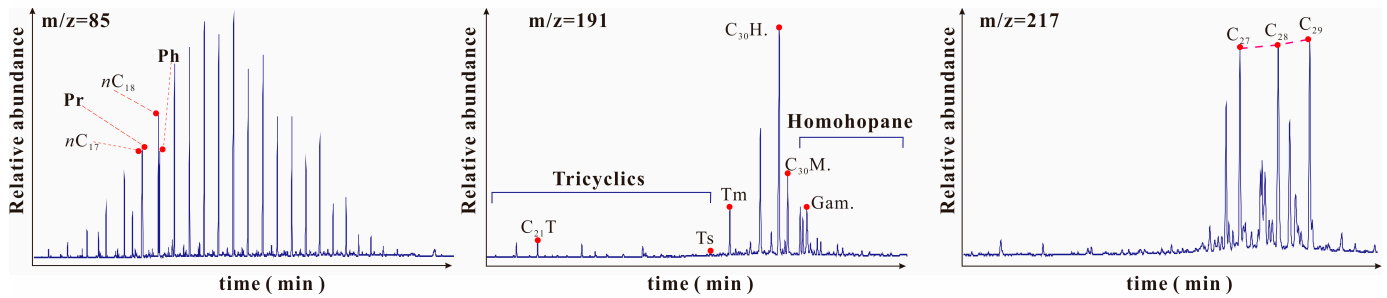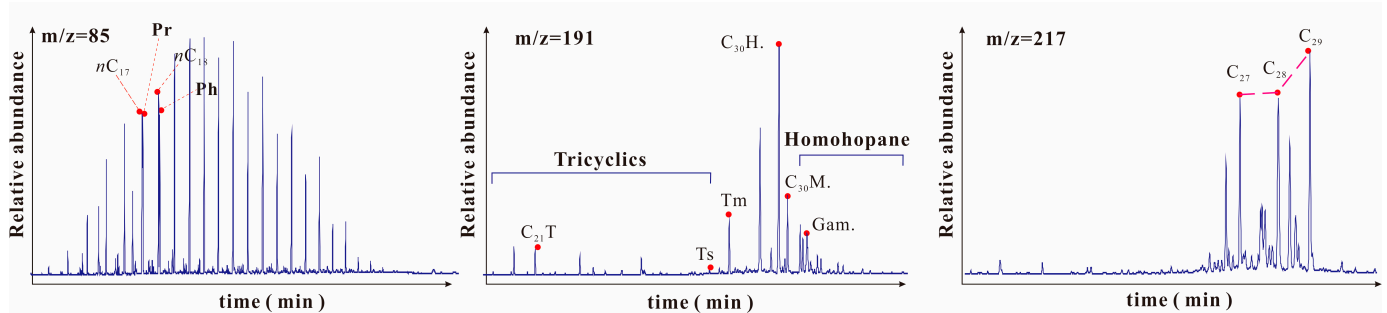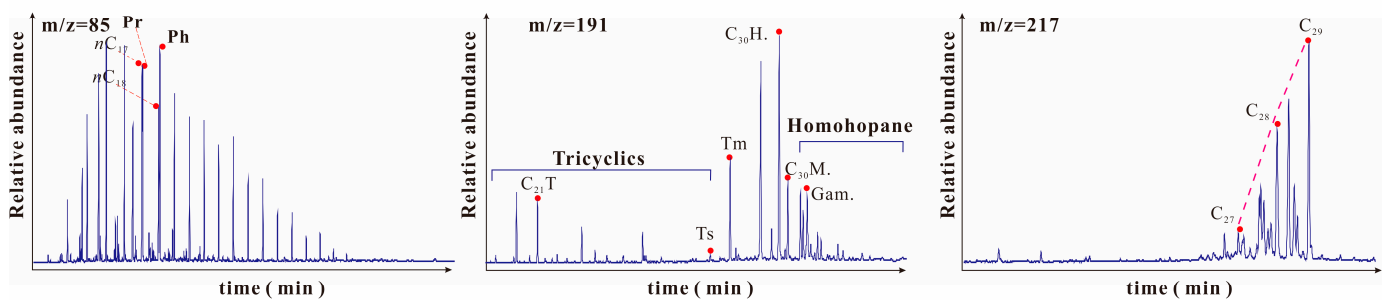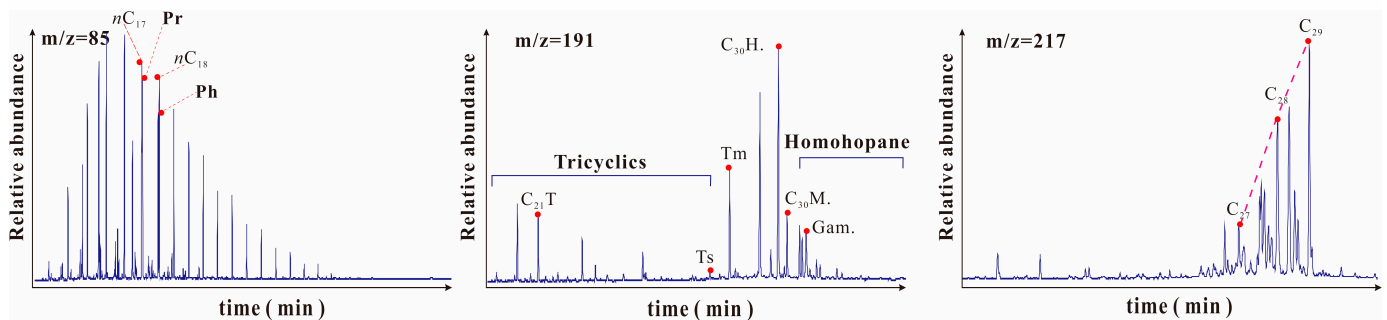
Figure 5. Typical biomarker spectrum of source rocks in the Lucaogou Formation of Well J305 in the Jimusar Sag. From left to right, the three columns show m/z 85, m/z 217, and m/z 191 distributions. C_{27} = C_{27}sterane 20R; C_{28} = C_{28}sterane 20R; C_{29} = C_{29}sterane 20R; C_{30}H. = C_{30}hopane; Gam. = Gammacerane; Ts = 18α(H)-22,29,30-trisnorneohopane; Tm = 17α(H)-22,29,30-trisnorhopane; Pr = pristine; Ph=phytane; C_{21}T = C_{21}tricyclic terpane.
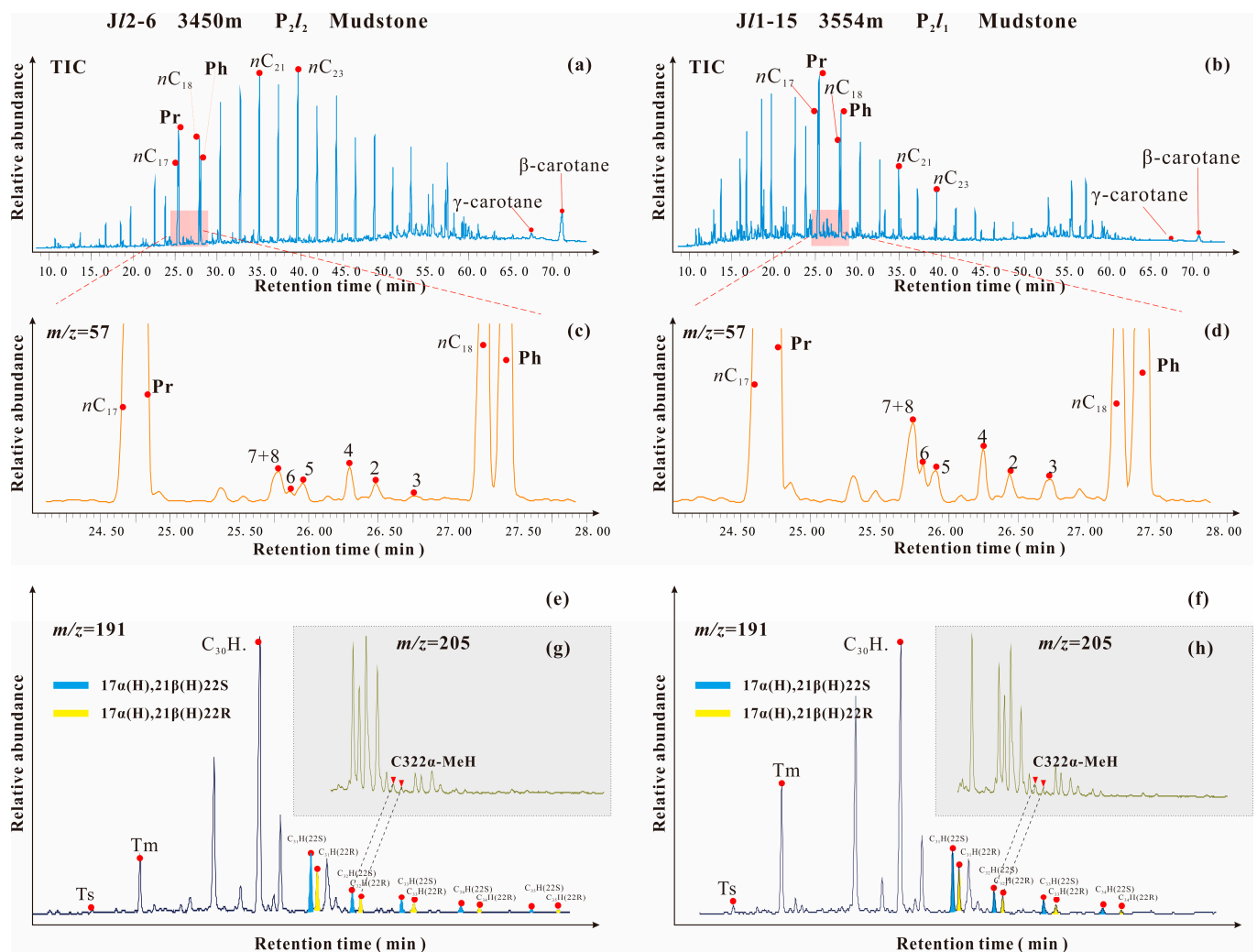
Figure 6. (**a**,**b**) TIC (total ion chromatograms) of samples Jl_2-6 and Jl_1-15, (**c**,**d**) m/z 57 mass fragmentograms showing the 7- + 8-C$_{18}$ Monomethyl alkanes of samples Jl_2-6 and Jl_1-15, (**e**,**f**) m/z 191 mass fragmentograms showing the hopanes distribution of samples Jl_2-6 and Jl_1-15, and (**g**,**h**) m/z 205 mass fragmentograms showing the 2α-methylhopane distributions of samples Jl_2-6 and Jl_1-15. MeH = methylhopanes.

4.2.3. Steranes

The relative abundance and distribution characteristics of steranes can be obtained with m/z 217 mass spectrum (Table 1; Figure 4). The proportion of C$_{29}$ sterane was relatively large (36.6~60.9%, average 50%), that of C$_{28}$ sterane was medium (22.1~40.4%, average 33%), and that of C$_{27}$ sterane was low (5.5~35.9%, average 17%). The C$_{29}$ sterane/C$_{27}$ sterane ratio in the P$_2l_2$ (1.2~5.4, average 2.1) was lower than that in the P$_2l_1$ (2.6~11.1, average 6.2).

4.3. Pyrolysis Simulation Experiments

The changes in the total oil production, expelled oil, and residual oil production rates of the samples (Jl_1-15 and Jl_2-6) are shown in Table 2. The gasses of the simulation experiment were mainly composed of two kinds of products, namely hydrocarbon gasses and non-hydrocarbon gasses. The hydrocarbon gasses mainly included alkanes such as CH$_4$, C$_2$H$_6$, and C$_3$H$_8$, while the non-hydrocarbon gasses were mainly N$_2$, H$_2$, CO$_2$, and CO (Table 2).

Table 2. Liquid and gaseous hydrocarbon yields of samples Jl_2-6 and Jl_1-15.

Sample	Pyrolysis Temperature (°C)	Liquid Hydrocarbon Yield (mg/g TOC)			Gaseous Hydrocarbon Yield (mg/g TOC)		
		Residual Oil	Expelled Oil	Total Oil	Total Hydrocarbon Gasses	Total Non-Hydrocarbon Gasses	Total Gasses
Jl_2-6	300	79.60	130.98	210.58	3.01	57.23	60.24
	350	182.61	293.00	475.61	30.11	66.55	96.66
	375	147.17	274.26	421.43	150.73	158.56	309.29
	400	92.35	218.89	311.24	310.00	230.98	540.98
	450	39.34	140.85	180.19	457.63	253.27	710.90
	500	19.15	65.29	84.44	535.04	294.63	829.67
Jl_1-15	300	90.43	155.26	245.69	0.80	76.58	77.38
	350	158.33	285.74	444.07	6.72	78.15	84.87
	375	245.13	343.21	588.34	73.57	176.50	250.07
	400	107.37	280.15	387.52	244.99	259.52	504.51
	450	64.60	149.22	213.82	406.00	297.93	703.93
	500	13.34	153.27	166.61	451.37	356.10	807.47

5. Discussion

5.1. Biomarker Characteristics of Source Rocks

5.1.1. Maturity of Organic Matter

The sterane isomerization parameters, such as 20S (%) (namely $C_{29}\alpha\alpha\alpha$ 20S/(20S + 20R)) and $\beta\beta$ (%) (namely $C_{29}\alpha\beta\beta/(\alpha\alpha\alpha + \alpha\beta\beta)$), have been widely used to characterize the thermal evolution of sediment organic matter during geological processes [38]. The variation ranges of 20S (%) and $\beta\beta$ (%) in the P_2l were 0.36~0.46 and 0.16~0.27, respectively, with average values of 0.42 and 0.22, respectively (Table 1; Figure 5). From the P_2l_1 to the P_2l_2, the 20S (%) and $\beta\beta$ (%) values decreased gradually. The variation trend of parameters reflects that the maturity of organic matter in the P_2l_1 was slightly higher than that of the P_2l_2. The organic matter maturity of the samples in the P_2l was basically low maturity to maturity, while that of the P_2l_1 was slightly higher (Figure 7). Based on the correlation between C_{29} sterane isomerization parameters and Ro [39], it is evident that the P_2l_2 samples had a Ro ranging from 0.6% to 0.8%, indicating that they originated from low-maturity source rocks. On the other hand, the Ro values of the P_2l_1 samples were around 0.7% to 0.8%, which suggests that they were sourced from mature rocks.
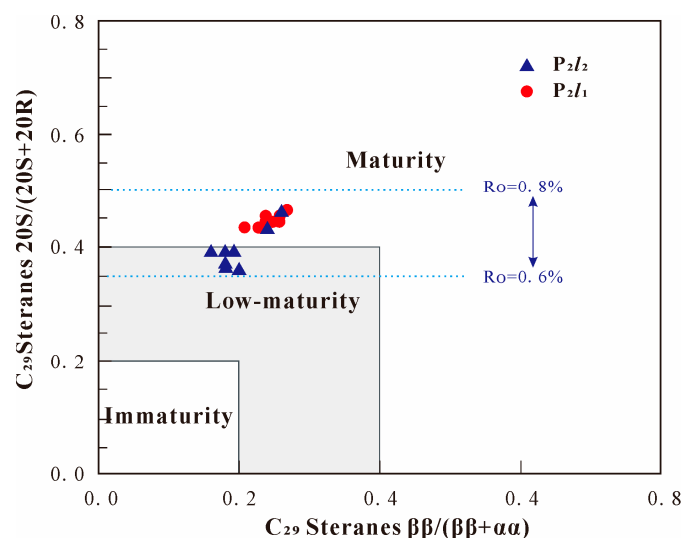

Figure 7. Maturity discrimination diagram of C_{29} sterane $\beta\beta/(\beta\beta + \alpha\alpha)$ versus $\alpha\alpha\alpha$ C_{29} sterane 20S/(20S + 20R) of the samples from Well J305 (Adapted with permission from Ref. [39]).

5.1.2. Sedimentary Environment of Organic Matter

The sedimentary environment of organic matter can be distinguished by the intersection diagram of the Ph/nC_{18} ratio and the Pr/nC_{17} ratio [40]. As shown in Figure 8, it

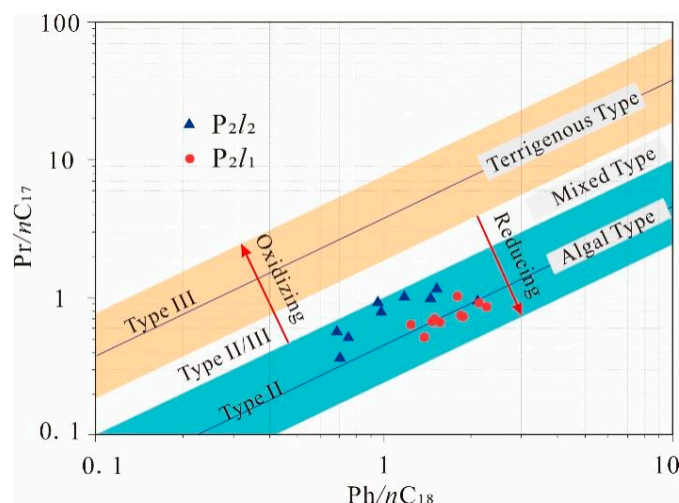shows that the sedimentary environment of the P_2l_1 was more anoxic and reductive than that of the P_2l_2.

Figure 8. Relationship between Pr/nC_{17} and Ph/nC_{18} ratio values for samples from the P_2l_1 and P_2l_2 (Adapted with permission from Ref. [40]).

Extended tricyclic terpenoids are derived from lipids in the prokaryotes of saline lakes [41]. Hence, in terms of organic geochemical parameters, ETR is a commonly used indicator to determine the salinity of water bodies in sedimentary environments [37]. The ETR values of the study samples ranged from 0.47 to 0.93, and decreased gradually from the P_2l_1 to the P_2l_2, indicating that the salinity of the P_2l_1 was higher than that of the P_2l_2 (Table 1; Figure 5).

5.1.3. Origin of Organic Matter

The abundance and correlation ratios of steranes are usually used to characterize the biological sources of organic matter [38]. The C_{27}-C_{28}-C_{29} sterane ternary diagram for the samples in this study shows that most of them had an aquatic plankton area (Figure 9).
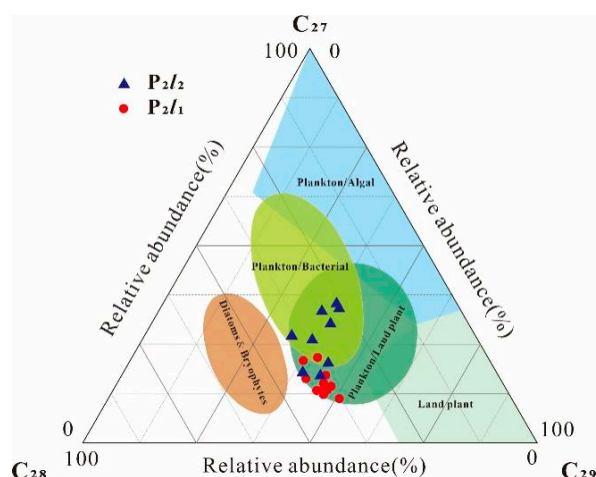

Figure 9. Ternary figure of C_{27}-C_{28}-C_{29} steranes in samples from the P_2l_1 and P_2l_2. (Adapted with permission from Ref. [42]).

Previous studies suggest that C_{29} sterane is mainly derived from terrestrial higher plants [43,44], while C_{28} steranes come from some phytoplankton, such as dinoflagellates, chlorella, diatoms, and brown algae, and may also come from green algae and higher plants [45]. Although C_{28} sterane can be synthesized by many algae and higher plants, the

above algae and higher plants only appear in large quantities after the Triassic, except for green algae [46,47]. Therefore, the C_{28} sterane in the source rocks of the Permian Lucaogou Formation (~280 Ma) was derived from green algae. C_{27} sterane is mainly derived from zooplankton and Rhodophyta [43,45]. The sterane proportions of all of the samples in the P_2l were C_{29} sterane (37~61%, with an average of 50%), followed by C_{28} sterane (22~40%, with an average of 33%), and the least was C_{27} sterane (5~35%, with an average of 17%), as shown in Figure 5. From the initial analysis, terrestrial higher plants were the main source of organic matter in the source rocks of the P_2l, followed by algae and bacteria, etc. However, C_{29} steroidal compounds can also be derived from cyanobacteria [48]. Taking into account the positive effects of volcanic-hydrothermal activities, volcanic ash can enrich surface water, and hydrothermal activities bring large amounts of nutrients that accelerate the development of phytoplankton and bacteria [7,25]. So, was the C_{29} sterane in this research primarily from terrestrial higher plants or from bacteria?

Firstly, the origin of the organic matter was analyzed by observing the peak type and the distribution pattern of the *n*-alkanes (Figure 4). The relative contents of bacteria, algae, and terrestrial higher plants in the organic matter of sediments can be analyzed by the relative abundance and the distributive patterns of *n*-alkanes. The main peak carbon number of bacteria and algae is less than nC_{21}, while the terrestrial higher plants are basically greater than nC_{27}, and the mixed source is in between them [49]. The main peak of *n*-alkane distribution in the source rocks of the P_2l_1 and P_2l_2 was ahead (Figure 4), reflecting that the abundance of terrestrial higher plants was lower than that of bacteria and algae.

Secondly, the *n*-alkanes above nC_{22+} are considered to be mainly derived from terrestrial higher plants, and the *n*-alkanes below nC_{21-} are considered to be mainly derived from plankton such as algae and bacteria [50]. In the P_2l_1, the nC_{21-}/nC_{22+} value was between 0.66 and 5.3, with a mean value of 2.52, while in the P_2l_2, the value was between 0.51 and 4.79, with a mean of 1.54 (Table 1). Obviously, the nC_{21-}/nC_{22+} values of the P_2l_1 were higher than that of the P_2l_2. The nC_{21-}/nC_{22+} values indicated that the organic matter in the P_2l may have mainly been derived from algae and bacteria, and the contribution of algae and bacteria to the organic matter in the P_2l_1 was greater. The S/H ratio (the ratio of steranes to hopanes) can reflect the relative ratio of algae (eukaryotes) to bacteria (prokaryotes) [51]. The S/H ratio of all of the samples ranged from 0.09 to 0.48, with an average of only 0.25 (Table 1). This reflects that the abundance of bacteria in organic matter, in which bacteria and algae are the main parent materials, was higher than that of algae.

In addition, in cyanobacteria culture and natural populations, some branched-chain monomethyl and dimethyl alkanes are often reported [52,53]. Predecessors have shown that cultured nostoc muscorum and anabaena variabilis (modern cyanobacteria) are rich in 7- and 8-carbon-substituted methylheptane [54]. The typical biomarker evidence of cyanobacteria hydrocarbon-generating parent material was medium-chain monomethyl alkanes [34], and the relative abundance can be indicated by the ratio of (7- + 8-MMAs)/C_{max}. 2α-methylhopane (2α-Meh) is a derivative of bacterial hopane polyol that is only found in cyanobacteria [55]. The ratio of 2α-methylhopane to hopanes (2α-C_{32}Meh/C_{32}H) represents the relative abundance of cyanobacteria compared to general bacteria [56]. As shown in Figure 4, the change trends in (7- + 8-C_{18}MMAs)/C_{max}, 2α-C_{32}MeH/C_{32}H and C_{29} sterane content in all of the samples were basically consistent. At the same time, the change trends in (7- + 8-C_{18}MMAs)/C_{max}, 2α-C_{32}MeH/C_{32}H and ETR values were also basically consistent, indicating the existence and evolution trend of cyanobacteria. From the P_2l_1 to the P_2l_2, with the decrease in salinity (ETR), the proportion of C_{29} sterane decreased, and the content of cyanobacteria decreased gradually. The abundance of cyanobacteria in the organic matter of the P_2l_1 was relatively high, while it was generally low in the P_2l_2.

Good exponential correlations between C_{29}/C_{27} sterane and (7- + 8-MMAs)/C_{max} values were observed ($R^2 = 0.68$) in the samples (Figure 10a). The $C_{22}T/C_{21}T$ ratio (C_{22} tricyclic terpane/C_{21} tricyclic terpane) can effectively determine the contribution of bacteria to the organic matter [49]. From the P_2l_1 to the P_2l_2, the ratio of $C_{22}T/C_{21}T$ values gradually decreased, and the value was positively correlated with C_{29} sterane (%) ($R^2 = 0.68$;

Figure 10b), and significantly negatively correlated with $C_{27}/(C_{27} + C_{29})$ sterane ($R^2 = 0.80$; Figure 10c). Therefore, the high proportion of C_{29} steranes (average 50%) in this study was most likely mainly derived from a mixture of bacteria (cyanobacteria) and terrestrial higher plants. The source of the C_{28} steranes (average 33%) was most likely green algae, and the C_{27} steranes (average 17%) were mainly derived from plankton, such as Rhodophyta.
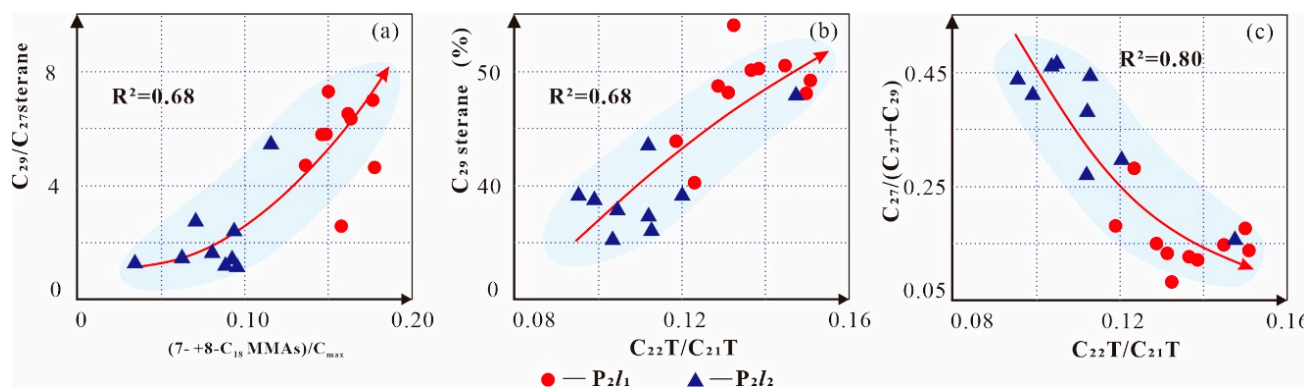

Figure 10. (**a**) the relationships between $(7- + 8\text{-MMAs})/C_{max}$ and C_{29}/C_{27} sterane; (**b**) the relationships between $C_{22}T/C_{21}T$ and C_{29} sterane (%); and (**c**) the relationships between $C_{22}T/C_{21}T$ and $C_{27}/(C_{27} + C_{29})$ sterane.

Based on the co-relation plots, it will be good to see if an estimate of the proportionate contribution of bacteria, algae, and terrestrial higher plants can be calculated. In summary, the overall characteristics of the biological source composition of the source rocks are that the abundance of bacteria and algae was greater than that of higher plants. Furthermore, the abundance of bacteria was greater than that of algae, of which the type was mainly green algae. As for the bacteria, cyanobacteria accounted for a certain proportion, and the proportion of cyanobacteria in the P_2l_1 was relatively high. From the P_2l_1 to the P_2l_2, the abundance of bacteria (including cyanobacteria) and algae (including green algae) decreased with the diminishing salinity.

5.1.4. Controlling Factors of Organic Matter Accumulation

Organic matter accumulation is controlled by primary productivity, the deposition rate, and the preservation conditions of sedimentary organic matter [12,57]. Biomarker parameters (such as sterane) can be used to effectively characterize the primary producers [37]. The variation trend of C_{27} sterane was opposite to that of TOC, while the variation trend of C_{28} sterane and C_{29} sterane was the same as that of TOC (Figure 5). Since C_{29} sterane and $C_{22}T/C_{21}T$ are related to $(7- + 8\text{-MMAs})/C_{max}$ (Figure 10), it can be speculated that the accumulation of organic matter during the deposition of the Lucaogou Formation was mostly related to the prosperity of bacteria (including a certain proportion of cyanobacteria) and algae.

In addition, G/H (gammacerane/$C_{30}\alpha\beta$ hopane) usually indicates the water layering, salinity, and an anoxic sedimentary environment [58]. There was a certain correlation between G/H and TOC ($R^2 = 0.61$), indicating that the water layering had a certain control effect on the organic matter accumulation (Figure 11a). The positive correlation between nC_{21-}/nC_{22+} and TOC indicates that the development of algae and plankton is beneficial to the enrichment of organic matter (Figure 11b). The Pr/Ph values were less than 1.0, indicating that the deposition process of the P_2l was mostly in the reduction condition, which is favorable for the preservation of organic matter. However, Pr/Ph has no correlation with TOC, indicating that the strength of reduction has little relationship with the enrichment of organic matter (Figure 11c). Through the analysis of the organic geochemical parameters combined with the volcanic-hydrothermal activity background, it is considered that the primary productivity heavily controls the accumulation of organic matter.
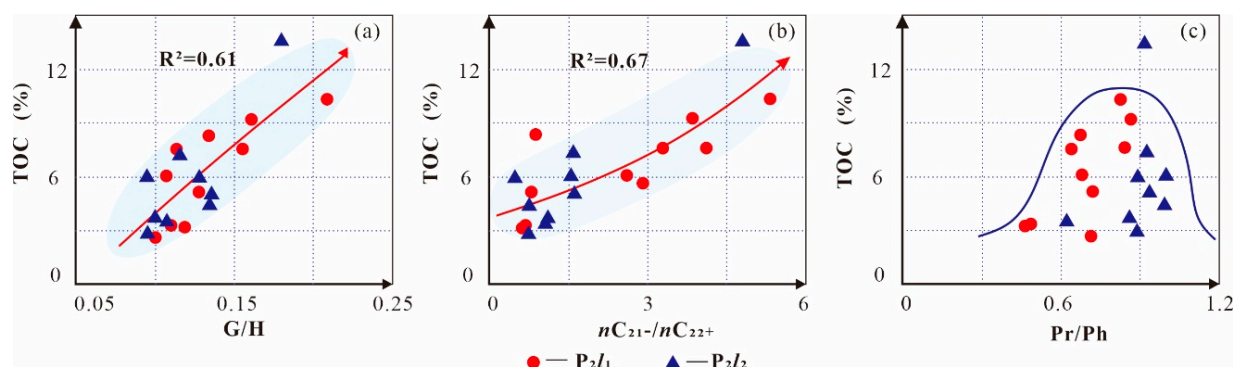
Figure 11. Correlations between TOC and biomarker parameters of the source rocks in P_2l. (**a**) Correlation between TOC and G/H (reflecting salinity and water stratification); (**b**) correlation between TOC and nC_{21-}/nC_{22+} (reflecting the sources of organic matter); and (**c**) correlation between TOC and Pr/Ph (representing redox strength).

5.2. Synergistic Evolution of Environment—Bionts of Source Rocks

The accumulation of organic matter in source rocks is largely influenced by primary productivity. However, the development of organic matter precursors is a crucial determinant in this process. The P_2l saline lake source rocks exhibited a coevolutionary relationship between bionts and the sedimentary environment. This relationship was primarily influenced by two environmental factors: salinity and water stratification. Biomarkers such as G/H and ETR are used to reflect these factors. G/H is indicative of water stratification, while ETR reflects the water salinity.

During the deposition period of the P_2l, the synergistic response of the water environment evolution and the biological compositions manifested in the positive correlation between the salinity index (ETR) and the S/H ratio (i.e., algae/bacteria ratio), $(C_{28} + C_{29} - St)/St$ (i.e., green algae/algae ratio), and $C_{22}T/C_{21}T$ (i.e., bacterial source) (Figure 12a–c). From the P_2l_1 to the P_2l_2, the proportion of bacteria (including a certain proportion of cyanobacteria) decreased with the diminishing salinity. The main sources of C_{27} sterane are plankton and Rhodophyta. C_{27} sterane is negatively correlated with ETR (salinity), and there is a threshold. When ETR < 0.7, it is conducive to the development of plankton and Rhodophyta (Figure 12d). With an increase in salinity, the proportion of green algae and bacteria increases, but the proportion of plankton and Rhodophyta decreases. Thus, it can be seen that the salinity of the water in the sedimentary period of the P_2l has a certain response to the composition of green algae, bacteria, plankton, and Rhodophyta in the source rocks.

5.3. Hydrocarbon Generation Potential of Source Rocks

5.3.1. Liquid Hydrocarbon Yields

For the sample (Jl_1-15) from the P_2l_1, the yields of expelled oil and residual oil were 343.21 mg/g TOC and 245.13 mg/g TOC, respectively, reaching a peak at 375 °C, and the total oil yield was 588.34 mg/g TOC. Being higher than 400 °C, the yields of expelled oil and residual oil showed a downward trend, but the yields of expelled oil slightly increased at 500 °C, relative to 450 °C (from 149.22 mg/g TOC to 153.27 mg/g TOC) (Figure 13). Meanwhile, a large amount of gas was produced, and the total hydrocarbon gas yield reached a peak of 451.37 mg/g TOC at 500 °C. For the sample (Jl_2-6) from the P_2l_2, the yields of expelled oil and residual oil reached a peak at 350 °C, which were 293.00 mg/g TOC and 182.61 mg/g TOC, respectively. In addition, the total oil yield was 475.61 mg/g TOC. At over 350 °C, the yields of expelled oil and residual oil showed a downward trend, and the yield of expelled oil did not increase compared to the upper member samples at 500 °C. The gas production rate increased rapidly over 375 °C, then, at 500 °C, the total hydrocarbon gas production rate reached 535.04 mg/g TOC.
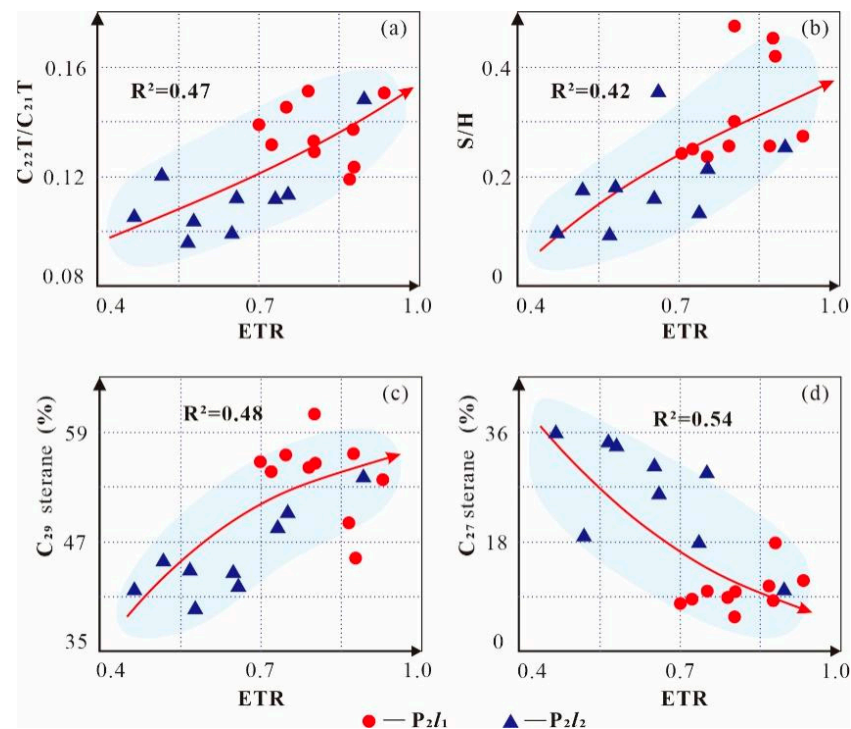
Figure 12. The correlation between the organic matter source and salinity in the source rocks of the P_2l. (**a**) Correlation between ETR and $C_{22}T/C_{21}T$; (**b**) correlation between ETR and S/H; (**c**) correlation between ETR and C_{29} sterane content; and (**d**) correlation between ETR and C_{27} sterane content.
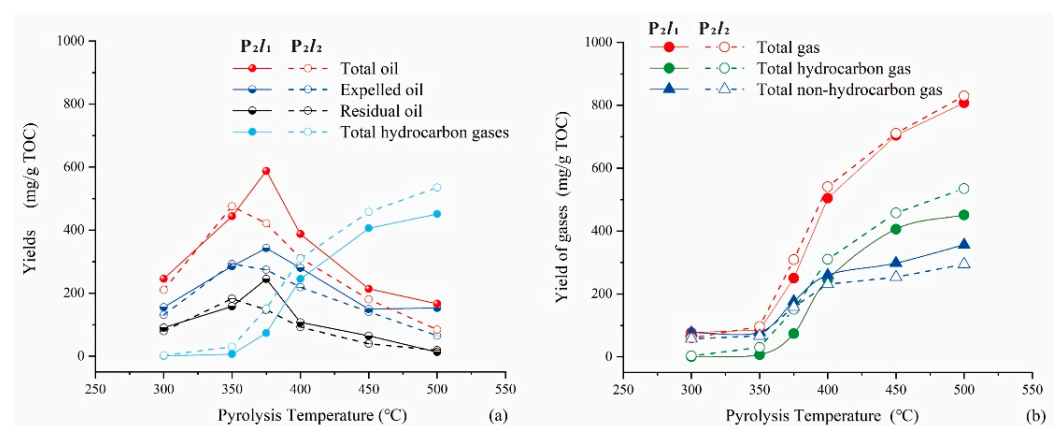

Figure 13. Sample Jl_1-15 (solid line) and sample Jl_2-6 (dotted line) oil and gas yield variations. (**a**) Liquid hydrocarbon and total hydrocarbon gas yield; and (**b**) gaseous hydrocarbon yield.

The peak temperatures of the oil production rate and the gas production rate were different for the samples from the P_2l_1 and the P_2l_2. The temperature points corresponding to the oil production peaks for the samples from the P_2l_2 and the P_2l_1 were 350 °C and 375 °C, respectively. The oil production rate of the P_2l_1 sample was higher, and there was a better oil-generation potential at 500 °C. However, the gas production rate of the P_2l_2 sample was higher.

5.3.2. Gaseous Hydrocarbon Yield

The total gas yields of the two samples from the P_2l_2 and the P_2l_1 increased with the raising of the simulation temperature. At 300 °C, the total gas yields of the Jl_2-6 and Jl_1-15 samples were 60.24 mg/g TOC and 77.38 mg/g TOC, respectively, and they reached 829.67 mg/g TOC and 807.47 mg/g TOC at 500 °C, respectivley, with little difference in total gas yields (Figure 13). The change in oil and gas production was composed of the following

two stages: (i) In the early stage of 300~350 °C, the hydrocarbon gas production rate of the Jl_2-6 and Jl_1-15 samples had little change, and the ranges of 3.01~30.11 mg/g TOC and 0.80~6.72 mg/g TOC changed, respectively. (ii) At over 375 °C, the hydrocarbon gas production rate increased rapidly, from 30.11 mg/g TOC and 6.72 mg/g TOC to 535.04 mg/g TOC and 451.37 mg/g TOC, respectively. It can be seen that the samples from the P_2l_2 had a higher hydrocarbon gas yield. The characteristics of the non-hydrocarbon gas yields of the two samples from the P_2l_2 and P_2l_1 are similar to those of hydrocarbon gasses. With the increase in the simulation temperature, they are also divided into two stages. Firstly, in the 300~350 °C stage, the yield ranges were 57.23~66.55 mg/g TOC and 76.58~78.15 mg/g TOC, respectively. Secondly, at 375~500 °C, the yield ranges were 158.56~294.63 mg/g TOC and 176.50~356.10 mg/g TOC, respectively. At the initial low-temperature stage, the yield of the non-hydrocarbon gas was higher than that of hydrocarbon gas, and the yield of non-hydrocarbon gas of the sample from the lower member was higher.

In summary, the biological compositions of the source rocks of the P_2l were impacted by water stratification and salinity, which reflects the co-evolution of the bionts and their environment. During the sedimentary period of the P_2l, there were frequent volcanic-hydrothermal activities that provided nutrients for the growth of organisms. These activities also resulted in changes in the salinity of the water body and improvements to the water stratification (Figure 14a). From the P_2l_1 to the P_2l_2, volcanic-hydrothermal activity and salinity decreased [7,59], the proportion of bacteria and green algae decreased, and the proportion of plankton and Rhodophyta increased. Figure 14b displays the trend of the ETR (salinity index) and 2α-C_{32}Meh/C_{32}H (cyanobacteria). Based on the differences in these indexes, the source rocks of the P_2l_1 and the P_2l_2 are classified into two types: HS-type (high salinity) and LS-type (low salinity).

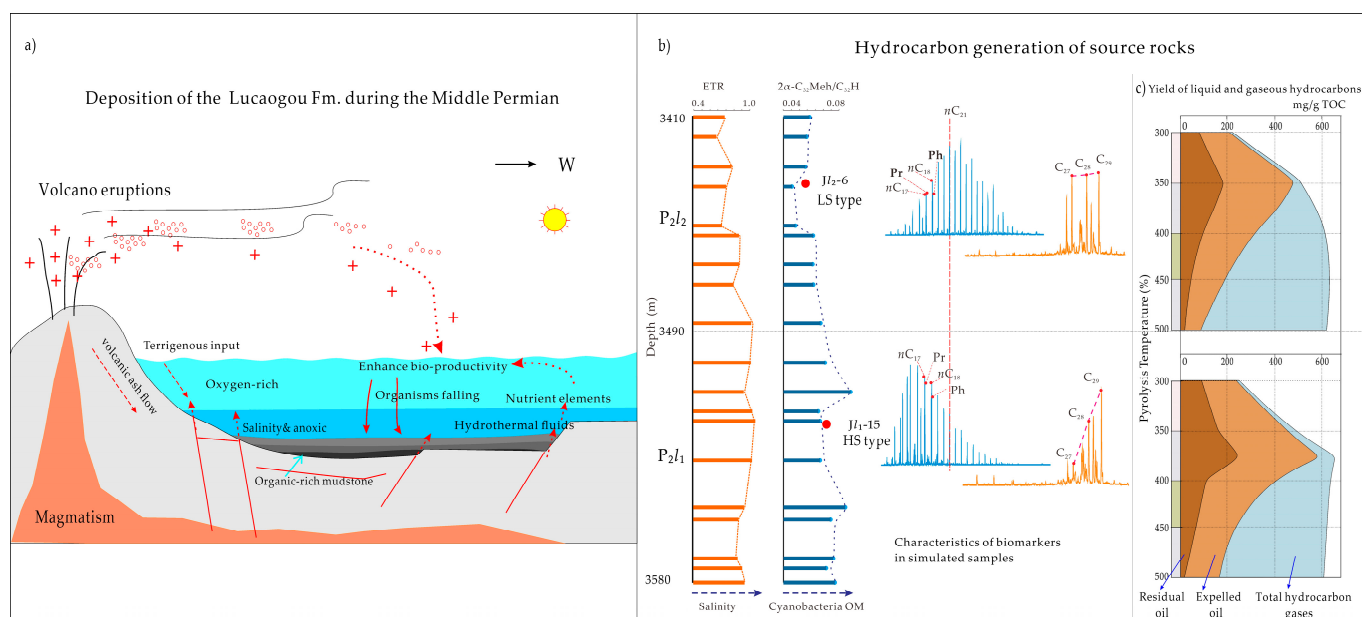**Figure 14.** (**a**) Schematic diagram of the paleoenvironmental conditions during deposition of the Lucaogou Formation in the Jimusar Sag; (**b**) a schematic diagram for the classification of source rock types; and (**c**) differences in the hydrocarbon generation potential of source rocks.

The source rocks of the P_2l_1 were formed in a high-salinity environment and can be classified as endmember HS-type. The organisms that were present in this environment mainly include green algae and bacteria. On the other hand, the source rocks of the P_2l_2 were formed in a low-salinity environment and can be classified as endmember LS-type. The organisms that were present in this environment mainly include plankton and Rhodophyta, and there may have been some input from higher plants (Figure 14b). The

interdependent relationship between the sedimentary environment and the bionts resulted in variations in the organic matter composition of the source rocks.

The source rock samples from the P_2l_1 and the P_2l_2 exhibited variations in their oil and gas generation potential (Figure 14c). In comparison to the LS-type source rocks, the HS-type source rocks had a higher tendency to produce oil, and the peak values of the liquid hydrocarbon yield were 588.34 mg/g TOC and 475.61 mg/g TOC, respectively (Table 2; Figure 7a). In comparison to the HS-type source rocks, the LS-type source rocks are known to produce a greater amount of gas. Specifically, the peak values for the gaseous hydrocarbon yield were 535.04 mg/g TOC for the LS-type rocks and 451.37 mg/g TOC for the HS-type rocks. (Table 2; Figure 7b). The difference in hydrocarbon generation potential between the P_2l_1 and the P_2l_2 may be attributed to the fact that the biological source of organic matter is influenced by changes in paleoenvironmental factors.

6. Conclusions

(1) During the sedimentary period of the Lucaogou Formation, the level of paleoproductivity played a crucial role in the enrichment of the organic matter. The biological source also co-evolved with the paleoenvironment to a certain extent. Specifically, the salinity of the sedimentary paleoenvironment had a significant impact on the prosperity of the algae and the bacteria.

(2) Compared to the LS-type source rocks (P_2l_2), the HS-type source rocks (P_2l_1) have a greater oil-generation potential, and their maximum oil generation peaks are 588.34 mg/g TOC (375 °C) and 475.61 mg/g TOC (350 °C), respectively. The maximum total hydrocarbon generation of the HS-type source rocks is slightly higher than that of the LS-type source rocks.

(3) The hydrocarbon generation parent material of the Lucaogou Formation may be controlled by the relative abundance of green algae and cyanobacteria, which is indicative to the Salt Lake Basin and affects the hydrocarbon generation potential of its source rocks. The source rocks that are formed in a high-salinity environment are derived from more cyanobacteria and may have better oil-generation potential.

Author Contributions: Conceptualization, Z.X. and H.T.; methodology, Z.L.; software, Y.Q.; validation, T.W. (Tao Wu), T.W. (Tianhai Wang), and Z.Q.; formal analysis, Z.X.; investigation, T.W. (Tianhai Wang) and D.M.; resources, H.T.; data curation, Z.X.; writing—original draft preparation, Z.X.; writing—review and editing, Z.X. and D.M.; visualization, L.S.; supervision, H.T.; project administration, Z.X.; funding acquisition, H.T. All authors have read and agreed to the published version of the manuscript.

Data Availability Statement: The data presented in this study are available upon request from the corresponding author. The data are not publicly available due to the need for further relevant research.

Conflicts of Interest: The authors declare no conflict of interest.

References

1. Kelts, K. Environments of deposition of lacustrine petroleum source rocks: An introduction. *Geol. Soc. Lond. Spec. Publ.* **1988**, *40*, 3–26. [CrossRef]
2. Carroll, A.R.; Brassell, S.C.; Graham, S.A. Upper Permian lacustrine oil shales, southern Junggar basin, northwest China. *AAPG Bull.* **1992**, *76*, 1874–1902. [CrossRef]
3. Qiu, Z.; Zou, C.N. Controlling factors on the formation and distribution of "sweet-spot areas" of marine gas shales in South China and a preliminary discussion on unconventional petroleum sedimentology. *J. Asian Earth Sci.* **2019**, *194*, 103989. [CrossRef]

4. Adegoke, A.K.; Abdullah, W.H.; Hakimi, M.H.; Yandoka, B.M.S. Geochemical characterisation of Fika Formation in the Chad (Bornu) Basin, northeastern Nigeria: Implications for depositional environment and tectonic setting. *Appl. Geochem.* **2014**, *43*, 1–12. [CrossRef]

5. Xia, L.W.; Cao, J.; Bian, L.Z.; Hu, W.X.; Wang, T.T.; Zhi, D.M.; Tang, Y.; Li, E.T. Co-evolution of paleo-environment and bio-precursors in a Permian alkaline lake, Mahu mega-oil province, Junggar Basin: Implications for oil sources. *Sci. China Earth Sci.* **2022**, *65*, 462–476. [CrossRef]

6. Keym, M.; Dieckmann, V.; Horsfield, B.; Erdmann, M.; Galimberti, R.; Kua, L.C.; Leith, L.; Podlaha, O. Source rock heterogeneity of the Upper Jurassic Draupne Formation, North Viking Graben, and its relevance to petroleum generation studies. *Org. Geochem.* **2006**, *37*, 220–243. [CrossRef]

7. Tao, H.F.; Qiu, Z.; Qu, Y.Q.; Liu, J.; Qin, Z.; Xie, Z.B.; Qiu, J.L.; Liu, B. Geochemistry of Middle Permian lacustrine shales in the Jimusar Sag, Junggar Basin, NW China: Implications for hydrothermal activity and organic matter enrichment. *J. Asian Earth Sci.* **2022**, *232*, 105267. [CrossRef]

8. Harris, N.B.; Freeman, K.H.; Pancost, R.D.; White, T.S.; Mitchell, G.D. The character and origin of lacustrine source rocks in the Lower Cretaceous synrift section, Congo Basin, west Africa. *AAPG Bull.* **2004**, *88*, 1163–1184. [CrossRef]

9. Ding, X.J.; Liu, G.D.; Zha, M.; Gao, C.H.; Huang, Z.L.; Qu, J.X.; Lu, X.J.; Wang, P.G.; Chen, Z.L. Geochemical characterization and depositional environment of source rocks of small fault basin in Erlian Basin, northern China. *Mar. Pet. Geol.* **2016**, *69*, 231–240. [CrossRef]

10. Liang, C.; Jiang, Z.; Cao, Y.C.; Wu, J.; Wang, Y.S.; Hao, F. Sedimentary characteristics and origin of lacustrine organic-rich shales in the salinized Eocene Dongying Depression. *Geol. Soc. Am. Bull.* **2018**, *130*, 154–174. [CrossRef]

11. Meyers, P.A.; Ishiwatari, R. Lacustrine organic geochemistry—An overview of indicators of organic matter sources and diagenesis in lake sediments. *Org. Geochem.* **1993**, *20*, 867–900. [CrossRef]

12. Arthur, M.A.; Dean, W.E. Organic-matter production and preservation and evolution of anoxia in the Holocene Black Sea. *Paleoceanography* **1998**, *13*, 395–411. [CrossRef]

13. Burdige, D.J. Preservation of organic matter in marine sediments: Controls, mechanisms, and an imbalance in sediment organic carbon budgets? *Chem. Rev.* **2007**, *107*, 467–485. [CrossRef]

14. Wu, H.G.; Hu, W.X.; Cao, J.; Wang, X.L.; Wang, X.L.; Liao, Z.W. A unique lacustrine mixed dolomitic-clastic sequence for tight oil reservoir within the middle Permian Lucaogou Formation of the Junggar Basin, NW China: Reservoir characteristics and origin. *Mar. Pet. Geol.* **2016**, *76*, 115–132. [CrossRef]

15. Wu, P.; Hou, D.J.; Gan, J.; Li, X.; Ding, W.J.; Gang, L.; Wu, B.B. Paleoenvironment and controlling factors of Oligocene source rock in the eastern deep-water area of the Qiongdongnan basin: Evidences from organic geochemistry and palynology. *Energy Fuels* **2018**, *32*, 7423–7437. [CrossRef]

16. Meyers, P.A. Organic geochemical proxies of paleoceanographic, paleolimnologic, and paleoclimatic processes. *Org. Geochem.* **1997**, *27*, 213–250. [CrossRef]

17. Kuang, L.C.; Hu, W.X.; Wang, X.L.; Wu, H.G.; Wang, X.L. Research of the Tight Oil Reservoir in the Lucaogou Formation in Jimusar Sag: Analysis of Lithology and Porosity Characteristics. *Geol. J. China Univ.* **2013**, *19*, 529–535. (In Chinese with English abstract) [CrossRef]

18. Jiang, Y.Q.; Liu, Y.Q.; Zhao, Y.; Nan, Y.; Wang, R.; Zhou, P.; Yang, Y.J.; Kou, J.Y.; Zhou, N.C. Characteristics and origin of tuff-type tight oil in Jimusaer sag, Junggar Basin, NW China. *Pet. Explor. Dev.* **2015**, *42*, 810–818. [CrossRef]

19. Uematsu, M.; Toratani, M.; Kajino, M.; Narita, Y.; Senga, Y.; Kimoto, T. Enhancement of primary productivity in the western North Pacific caused by the eruption of the Miyake-jima Volcano. *Geophys. Res. Lett.* **2004**, *31*, 177–182. [CrossRef]

20. Duggen, S.; Croot, P.; Schacht, U.; Hoffmann, L. Subduction zone volcanic ash can fertilize the surface ocean and stimulate phytoplankton growth: Evidence from biogeochemical experiments and satellite data. *Geophys. Res. Lett.* **2007**, *34*, 95–119. [CrossRef]

21. Wang, X.Q.; Sun, L.; Zhu, R.K.; Jin, X.; Li, J.M.; Wu, S.T.; Bi, L.N.; Liu, X.D. Application of charging effects in evaluating storage space of tight reservoirs: A case study from Permian Lucaogou Formation in Jimusar sag, Junggar Basin, NW China. *Pet. Explor. Dev.* **2015**, *42*, 516–524. [CrossRef]

22. Zhang, D.W.; Wang, L.H.; Su, L.; Wu, Y.D.; Sun, R.; Wu, C.J.; Song, D.J.; Tuo, J.C. The chemical kinetics of the semi-open hydrous pyrolysis system: Time series analysis of lithostatic pressure and fluid pressure. *Int. J. Coal Geol.* **2020**, *220*, 103418. [CrossRef]

23. Kuang, L.C.; Wang, X.T.; Guo, X.G.; Chang, Q.S.; Jia, X.Y. Geological characteristics and exploration practice of tight oil of Lucaogou Formation in Jimsar Sag. *Xinjiang Pet. Geol.* **2015**, *36*, 629–634, (In Chinese with English abstract). [CrossRef]

24. Xie, Z.B.; Qu, Y.Q.; Wu, T.; Wang, T.H.; Liu, Y.T.; Hei, C.L.; Tao, H.F. Discussion on the sedimentary paleoenvironment and biological source of Permian Lucaogou Formation in Jimusar Sag, Junggar Basin. *Nat. Gas Geosci.* **2023**, *6*. Available online: http://kns.cnki.net/kcms/detail/62.1177.TE.20230218.2248.002.html (accessed on 11 February 2023). (In Chinese).

25. Cao, Z.; Liu, G.D.; Xiang, B.L.; Wang, P.; Niu, G.; Niu, Z.C.; Li, C.Z.; Wang, C.Y. Geochemical characteristics of crude oil from a tight oil reservoir in the Lucaogou Formation, Jimusar sag, Junggar Basin. *AAPG Bull.* **2017**, *101*, 39–72. [CrossRef]

26. Cao, Z.; Liu, G.D.; Zhan, H.B.; Gao, J.; Zhang, J.Y.; Li, C.Z.; Xiang, B.L. Geological roles of the siltstones in tight oil play. *Mar. Pet. Geol.* **2017**, *83*, 333–344. [CrossRef]

27. Qiu, Z.; Wu, X.Z.; Tang, Y.; Zheng, M.; Wang, G.J.; Guo, Q.L.; Wang, S.J.; Xie, H.B. Resource Assessment of Tight Oil from the Permian Lucaogou Formation in Jimusar Sag, Junggar Basin, China. *Nat. Gas Geosci.* **2016**, *27*, 1688–1698, (In Chinese with English abstract). [CrossRef]

28. Zhang, S.M. Diagenesis and Genetic Mechanism of Tight Oil Reservoir of the Permian Lucaogou Formation, Jimusar Sag, China. Ph.D. Thesis, China University of Petroleum (East China), Beijing, China, 2019. [CrossRef]

29. Song, D.J.; Wu, C.J.; Chen, K.; Zhang, M.F.; He, W.; Su, L.; Zhang, D.W.; Fu, S.; Tuo, J.C. Gas Generation from Marine and Terrestrial Shales by Semi-Closed Pyrolysis Experiments. *Earth Sci.* **2019**, *44*, 3639–3652. [CrossRef]

30. Fang, S.H.; Xu, H.M.; Song, Y.; Li, J.M.; Liu, L.J.; Zhang, J. Characteristics and evolution of the composite petroleum system in Jimusar depression, eastern Junggar Basin. *Acta Geosci. Sin.* **2005**, *3*, 259–264. [CrossRef]

31. Qiu, N.S.; Yang, H.B.; Wang, X.L. Tectono-thermal evolution in the Junggar Basin. *Chin. J. Geol.* **2002**, *4*, 423–429. [CrossRef]

32. Wang, J.; He, K.; Zhi, W.D.; Wang, Z.; Wang, L. Characteristics of temperature and pressure fields in Zhundong area, Junggar Basin. *Xinjiang Pet. Geol.* **2010**, *31*, 51–53. [CrossRef]

33. Song, D.J.; Tuo, J.C.; Zhang, M.F.; Wu, C.J.; Su, L.; Li, J.; Zhang, Y.H.; Zhang, D.W. Hydrocarbon generation potential and evolution of pore characteristics of Mesoproterozoic shales in north China: Results from semi-closed pyrolysis experiments. *J. Nat. Gas Sci. Eng.* **2019**, *62*, 171–183. [CrossRef]

34. Shiea, J.; Brassell, S.C.; Ward, D.M. Mid-chain branched mono-and dimethyl alkanes in hot spring cyanobacterial mats: A direct biogenic source for branched alkanes in ancient sediments? *Org Geochem.* **1990**, *15*, 223–231. [CrossRef]

35. Luo, G.M.; Hallmann, C.; Xie, S.C.; Ruan, X.Y.; Summons, R.E. Comparative microbial diversity and redox environments of black shale and stromatolite facies in the Mesoproterozoic Xiamaling Formation. *Geochim. Cosmochim. Acta* **2015**, *151*, 150–167. [CrossRef]

36. Ding, W.J.; Hou, D.J.; Jiang, L.; Jiang, Y.H.; Wu, P. High abundance of carotanes in the brackish-saline lacustrine sediments: A possible cyanobacteria source? *Int. J. Coal Geol.* **2020**, *219*, 103373. [CrossRef]

37. Hao, F.; Zhou, X.H.; Zhu, Y.M.; Yang, Y.Y. Lacustrine source rock deposition in response to co-evolution of environments and organisms controlled by tectonic subsidence and climate, Bohai Bay Basin, China. *Org. Geochem.* **2011**, *42*, 323–339. [CrossRef]

38. Seifert, W.K.; Moldowan, J.M. The effect of thermal stress on source-rock quality as measured by hopane stereochemistry. *Phys. Chem. Earth* **1980**, *12*, 229–237. [CrossRef]

39. Justwan, H.; Dahl, B.; Isaksen, G.H. Geochemical characterisation and genetic origin of oils and condensates in the South Viking Graben, Norway. *Mar. Pet. Geol.* **2006**, *23*, 213–239. [CrossRef]

40. Connan, J.; Cassou, A.M. Properties of gases and petroleum liquids derived from terrestrial kerogen at various maturation levels. *Geochem. Cosmochim. Acta* **1980**, *44*, 1–23. [CrossRef]

41. De Grande, S.M.B.; Neto, F.R.A.; Mello, M.R. Extended tricyclic terpanes in sediments and petroleums. *Org. Geochem.* **1993**, *20*, 1039–1047. [CrossRef]

42. Huang, W.Y.; Meinschein, W.G. Sterols as ecological indicators. *Geochem. Cosmochim. Acta* **1979**, *43*, 739–745. [CrossRef]

43. Shi, J.Y.; Mackenzie, A.S.; Alexander, R.; Eglinton, G.; Gowar, A.P.; Wolff, G.A.; Maxwell, J.R. A biological marker investigation of petroleum and shales from the Shengli oilfield, the People's Republic of China. *Chem. Geol.* **1982**, *35*, 1–31. [CrossRef]

44. Knoll, A.H.; Summons, R.E.; Waldbauer, J.R.; Zumberge, J.E. The geological succession of primary producers in the oceans. In *Evolution of Primary Producers in the Sea*; Academic Press: Cambridge, MA, USA, 2007; pp. 133–163. [CrossRef]

45. Volkman, J.K. A review of sterol markers for marine and terrigenous organic matter. *Org. Geochem.* **1986**, *9*, 83–99. [CrossRef]

46. Damsté, J.S.S.; Muyzer, G.; Abbas, B.; Rampen, S.W.; Masse, G.; Allard, W.G.; Belt, S.T.; Robert, J.M.; Rowland, S.J.; Moldowan, J.M.; et al. The rise of the rhizosolenid diatoms. *Science* **2004**, *304*, 584–587. [CrossRef] [PubMed]

47. Müller, M.N. On the genesis and function of coccolithophore calcification. *Front. Mar. Sci.* **2019**, *6*, 49. [CrossRef]

48. Volkman, J.K.; Barrett, S.M.; Blackburn, S.I.; Mansour, M.P.; Sikes, E.L.; Gelin, F. Microalgal biomarkers: A review of recent research developments. *Org. Geochem.* **1998**, *29*, 1163–1179. [CrossRef]

49. Peters, K.E.; Walters, C.C.; Moldowan, J.M. *The Biomarker Guide: Biomarkers and Isotopes in Petroleum Exploration and Earth History*; The Press Syndicate of the University of Cambridge: Cambridge, MA, USA, 2005; Volume 2.

50. Tissot, B.P.; Welte, D.H. *Petroleum Formation and Occurrence*, 2nd ed.; Springer: Berlin/Heidelberg, Germany, 1984.

51. Rohrssen, M.; Love, G.D.; Fischer, W.; Finnegan, S.; Fike, D.A. Lipid biomarkers record fundamental changes in the microbial community structure of tropical seas during the Late Ordovician Hirnantian glaciation. *Geology* **2013**, *41*, 127–130. [CrossRef]

52. Boudou, J.P.; Espitalié, J. Molecular nitrogen from coal pyrolysis: Kinetic modeling. *Chem. Geol.* **1995**, *126*, 319–333. [CrossRef]

53. Boudou, J.P.; Trichet, J.; Robinson, N.; Brassell, S.C. Profile of Aliphatic Hydrocarbons in a Recent Polynesian Microbial Mat. *Int. J. Environ. Anal. Chem.* **1985**, *26*, 137–155. [CrossRef]

54. Kenig, F.; Damsté, J.S.S.; Kock-van Dalen, A.C.; Rijpstra, W.I.C.; Huc, A.Y.; De Leeuw, J.W. Occurrence and origin of mono-, di-, and trimethylalkanes in modern and Holocene cyanobacterial mats from Abu Dhabi, United Arab Emirates. *Geochim. Cosmochim. Acta* **1995**, *59*, 2999–3015. [CrossRef]

55. Summons, R.E.; Jahnke, L.L.; Hope, J.M.; Logan, G.A. 2-Methylhopanoids as biomarker for cyanobacterial oxygenic photosynthesis. *Nature* **1999**, *400*, 554–557. [CrossRef]
56. Xie, S.; Pancost, R.D.; Yin, H.; Wang, H.; Evershed, R.P. Two episodes of microbial change coupled with Permo/Triassic faunal mass extinction. *Nature* **2005**, *434*, 494–497. [CrossRef]
57. Calvert, T.F. Anoxia vs. productivity: What controls the formation of organic carbon rich sediments and sedimentary rocks? *AAPG Bull.* **1990**, *74*, 454–466. [CrossRef]
58. Haven, H.L.T.; Rohmer, M.; Rullkötter, J.; Bisseret, P. Tetrahymanol, the most likely precursor of gammacerane, occurs ubiquitously in marine sediments. *Geochem. Cosmochim. Acta* **1989**, *53*, 3073–3079. [CrossRef]
59. Zhang, S.M.; Cao, Y.C.; Liu, K.Y.; Jahren, J.; Xi, K.L.; Zhu, R.K.; Yang, T.; Cao, X.; Wang, W. Characterization of lacustrine mixed fine-grained sedimentary rocks using coupled chemostratigraphic-petrographic analysis: A case study from a tight oil reservoir in the Jimusar Sag, Junggar Basin. *Mar. Pet. Geol.* **2019**, *99*, 453–472. [CrossRef]